Magnetic Resonance Imaging 57 (2019) 218–234

Contents lists available at ScienceDirect

Magnetic Resonance Imaging

journal homepage: www.elsevier.com/locate/mri

Original contribution

Fiber orientation distribution function from non-negative sparse recovery with quantitative analysis of local fiber orientations and tractography using DW-MRI datasets

Thinhinane Megherbi[a,*], Gabriel Girard[b], Aurobrata Ghosh[c,1], Fatima Oulebsir-Boumghar[a], Rachid Deriche[c]

[a] ParIMéd/LRPE,FEI,USTHB, BP 32 El Alia, Bab Ezzouar 16111, Algiers, Algeria
[b] Signal Processing Lab (LTS5), École Polytechnique Fédérale de Lausanne, Lausanne, Switzerland
[c] Athena Project-Team, Inria Sophia Antipolis-Méditerranée, Université Côte d'Azur, France

ARTICLE INFO

Keywords:
DW-MRI
Fiber orientation distribution (FOD) function
Tensors
Symmetric tensor decomposition
Sparsity
Non-negative least square
Tractography
Tractometer

ABSTRACT

Diffusion weighted MRI (DW-MRI) is the unique non-invasive imaging modality capable of estimating in vivo the structure of the white matter. In this paper, we propose, evaluate and validate a new DW-MRI method to model and recover high quality tractogram even with multiple fiber populations in a voxel and from a limited number of acquisitions.

Our method relies on the estimation of the Fiber Orientation Distribution (FOD) function, parameterized as a non-negative sum of rank-1 tensors and the use of a non-negative sparse recovery scheme to efficiently recover the tensors, and their number. Each fiber population of a voxel is characterized by the orientation and the weight of a rank-1 tensor.

Using both deterministic and probabilistic tractography algorithms, we show that our method is able to accurately reconstruct narrow crossing fibers and obtain a high quality connectivity reconstruction even from a limited number of acquisitions. To this end, a validation scheme based on the connectivity recovered from tractography is developed to quantitatively evaluate and analyze the performance of our method. The tractometer tool is used to quantify the tractography obtained from a simulated DW-MRI dataset including a high angular resolution dataset of 60 gradient directions and a dataset of 30 gradient directions, each of them corrupted with Rician noise of SNR 10 and 20. The performance of our FOD model and its impact on the tractography results are also demonstrated and illustrated on in vivo DW-MRI datasets with high and low angular resolutions.

1. Introduction

The diffusion weighted magnetic resonance imaging or DW-MRI [1] is a substantial advance in neuroimaging since it reveals the neuronal architecture of the brain white matter (WM) in vivo and non-invasively. The DW-MRI technique quantifies the free and constrained motion of the water molecules in the neuronal fibers. The first model used to reconstruct these fiber bundles was the second order diffusion tensor (DTI) introduced by Basser et al. in 1994 [2]. This model requires a low number of acquisitions, but does not correctly represent the diffusion signal in the many regions where the WM fiber bundles intersect [2]. To overcome these limitations, novel high angular resolution imaging techniques (HARDI) have been proposed, such as the diffusion spectrum imaging (DSI) and the Q-Ball imaging (QBI) commonly used in practice [3-5]. From these HARDI acquisitions, we can model the diffusion profile with spherical functions, like the diffusion orientation distribution function (ODF) or the fiber orientation distribution (FOD) function. Both of these functions resolve the crossing fibers problem by having their local maxima aligned on the orientations of the underlying fiber bundles. However, the angular resolution of the ODF function is limited as it fails to reconstruct correctly crossing fibers when angles are less than 60° approximately [6,7]. The FOD function has a more sharper profile allowing an angular resolution gain up to 15° [8]. The state of art FOD algorithm reconstructs the WM fibers from a spherical deconvolution of the DW-MRI signal [9-17]. Traditionally, the FOD function is described in spherical harmonics (SH) basis, where the

* Corresponding author.
E-mail address: tmegherbi@usthb.dz (T. Megherbi).
[1] AI Innovation Lab, Verisk Analytics, Munich, Germany. From November 2017.

https://doi.org/10.1016/j.mri.2018.10.003
Received 25 May 2018; Received in revised form 6 October 2018; Accepted 6 October 2018

acuteness of the angular resolution directly depends on the order of the SH basis. Consequently, a high number of acquisitions can be required. In higher orders case, the FOD is prone to negatives lobes due to noise, which has no physical meaning. This can be partially countered by imposing a non-negativity constraint, as in the constrained spherical deconvolution model (CSD) [9], the *super resolved CSD* model [9] or in *non-negative SD* method (NNSD) [10].

To impose elegantly the positivity constraint, high order symmetric tensors (HOT) or equivalently homogeneous polynomials were proposed recently to model the FOD function in the spherical deconvolution formulation, so-called CT-FOD for Cartesian tensor-FOD [15]. As the FOD described in the SH basis, this non-negative Cartesian tensor has its local maxima aligned on the orientations of the underlying fibers.

Considering that only a small number of the FOD values are non-zero, sparse SD methods [11,14,16-18] were recently proposed to reconstruct the FOD. In Ref. [16], the authors exploited the compress sensing mathematical framework and proposed to reformulate the SD problem as a reweighted constrained l_1 minimisation with the aim to exploit the sparsity more optimally. This method requires predefining the number of fiber compartments in each voxel. Feng et al. [17] enforces the sparse constraints on the FOD represented in the high order tensors basis, by applying both the l_1 and l_2 norms in the SD problem.

When the FOD is represented in the SH basis like the CSD which remains the widely used method, an exhaustive search of the local maxima is generally performed to recover the local fiber orientations; while the polynomial form of the Cartesian tensor FOD allows to recover the fiber orientations by local maxima extraction using either the Z-eigenvalues concept [19-21] or the high order tensors decomposition [22-25]. However, the Z-eigenvalues method doesn't recover crossing fibers at angles below 60° [26] from fourth order tensor. The tensor decomposition improves the angular resolution [25] and the first algorithm used for the fibers orientations detection issue was the low-rank decomposition approximation method known as CANDCOMP/PARAFAC [22-24,27], in the following we will refer to this method by PARAFAC. This numerical PARAFAC-decomposition approximation algorithm doesn't give a minimal decomposition and requires predefining the tensor rank corresponding to the number of the underlying fibers, which is impossible a priori. A recent method called Adecomp-SHOT for Analytical decomposition of symmetric high order tensor, proposed in 2014 [25] solves the tensor decomposition problem analytically and unlike the PARAFAC-decomposition approximation, this approach is not restricted to sub-generic ranks and provides a minimal decomposition without any prior information. Nevertheless, these previous methods make the correspondence between the tensor decomposition and the fiber-orientations, even though there exists no explanation to justify this physical modelling.

The objective of this paper is to complete our work, firstly introduced in ISBI [28], to show how to physically model the fiber orientations corresponding to oriented delta functions using high order rank-1 tensors and present a newly and advanced validation framework developed to quantitatively evaluate and analyze the performance of our method. Thus, in this method the spherical deconvolution problem is revisited by modelling the FODs initially with tensors that are decomposable into positive sums of rank-1 tensors instead of estimating FODs in the SH basis or as non-negative tensors and then solving the problem of tensor decomposition. In this new FOD model, the tensor order can be chosen arbitrarily high without increasing the number of unknowns i.e. without requiring more information which correspond to the number of acquisitions or gradient directions. Thus, in this method we propose a novel technique based on non-negative sparse recovery scheme to estimate simultaneously sharp positive-definite FODs, the fibers orientations and the number of underlying crossing fibers from limited number of acquisitions. In the remainder of the paper, we refer to this FOD from non-negative sparse recovery by spFOD.

Thus, among several spherical deconvolution techniques, the FODs can be estimated using the CSD model, as a non-negative tensor using the CT-FOD model or by a sum of non-negative rank-1 tensors using our new spFOD model. To date, the CSD is the most popular model of the FOD and the commonly used in practice [3-5]. Unlike the spFOD method, the CSD and the CT-FOD methods require an additional step to recover the fiber orientations using exhaustive localisation on sphere, Z-eigenvalues concept or tensor decomposition methods. Usually, these fiber orientations detecting techniques are evaluated and compared to the state of art based only on local measurements of the angular resolution and accuracy. However, one of the major goal of DW-MRI techniques is the reconstruction of accurate tractogram of the brain white matter using tractography algorithms. Therefore, in this paper we evaluate the local fiber orientations reconstruction methods on the basis of the accuracy of the global resulted connectivity. Thus, the originality of this work consists in an advanced evaluation and validation of our spFOD method and comparing it to the state of art algorithms based on the tractography results, where we analyze quantitatively the resulted connectivity using the tractometer tool [29]. To highlight the efficiency of our spFOD, we conduct tests with both HARDI simulated DW-MRI data and low angular resolution data, corrupted with a Rician noise of different SNR. Furthermore, we analyze the results of both deterministic and probabilistic tractography. Finally, qualitative tests on in vivo DW-MRI dataset of different number of acquisitions, reveal how our spFOD method correctly extracts the crossing fibers orientations from limited number of acquisitions.

2. Material and methods

2.1. FOD from spherical deconvolution

Under the assumption that the diffusion characteristics are approximately constant (similar diffusion profile) for all fiber bundles, the fibers orientations distribution within a voxel can be estimated using the spherical deconvolution operation. Thus, the HARDI signal $S(\theta,\phi)$, with (θ,ϕ) the spherical coordinates, is given by a convolution (*) over a sphere of the response function $R(\theta)$ representing the signal measured from a single fiber voxel, with the FOD function $F(\theta,\phi)$ [9], as illustrated by Fig. 1.

$$S(\theta, \phi) = R(\theta)*F(\theta, \phi) \quad (1)$$

The FOD contains all the information about the fiber orientations, which are indirectly modelled as oriented Dirac delta functions. These

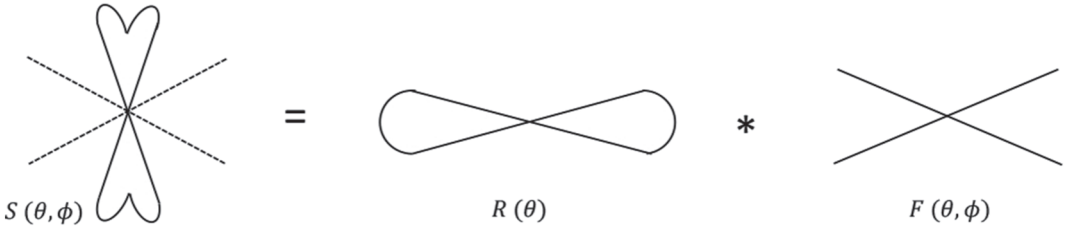

Fig. 1. Spherical deconvolution. FOD: sum of oriented Dirac delta functions. (Inspired from Ref. [30]).

fiber orientations and the FOD function are estimated by deconvolving the response function $R(\theta)$ from the raw signal $S(\theta,\phi)$. The spherical deconvolution operation is traditionally performed in the spherical and rotational harmonics basis. In these basis, the convolution operation is reduced to a simple one matrix multiplication per harmonic order [9]:

$$\mathbf{S}_l = \mathbf{F}_l . \mathbf{R}_l \tag{2}$$

with l being the harmonic order, $\mathbf{S}_l$ and $\mathbf{F}_l$ are vectors of length $2l + 1$ containing the SH coefficients of the raw signal and the FOD respectively. Whereas, the response function is represented using the rotational harmonics [31] and its coefficients are written as a matrix $\mathbf{R}_l$ of size $(2l + 1) \times (2l + 1)$. Then, the SH coefficients of the FOD function can be calculated with a simple matrix inversion.

The spherical deconvolution problem posed in Eq. (2) is susceptible to noise which induces negative values on the sphere. The first approach proposed to minimise the effect of this noise at the cost of the angular resolution was the introduction of a low-pass filter to attenuate the high angular frequency components in the FOD that appear as spurious negative lobes, this method is called the *filtered SD* [30]. However, eliminating systematically these high frequencies induces a loss of the angular information affecting the angular resolution. Constrained methods like the CSD and its variant the *super resolved CSD* [9] were proposed to estimate the FOD in the SH representation by imposing a constraint on the presence of negative values in the FOD, without affecting the angular resolution.

The CSD method is an iterative process that considers an initial estimate of the FOD using the filtered SD, then estimate an improved FOD using a constrained Tikhonov regularisation commonly used for ill-posed problems. This consists in incorporating in the regularisation a constraint on the presence of a set of directions along which the amplitude of the FOD is below a threshold τ. In practice, this last one is set to 10% of the mean FOD amplitude [9].

At each iteration, a new set of these directions are identified and an improved FOD is estimated, the procedure is repeated until the convergence is achieved. The CSD problem is thus described by a constraint minimisation of a weighted sum of two terms, involved by the Tikhonov regularisation:

$$f_{i+1} = \arg\min\{\|\mathbf{A}f_i - \mathbf{b}\|^2 + \lambda^2\|\mathbf{L}f_i\|^2\} \tag{3}$$

In the first term of the sum, **A** represents the problem matrix describing the spherical deconvolution with **R**, response function, in the spherical harmonic basis [9], f_i represents the current estimate of the SH coefficients of the FOD and **b** being the raw signal values. The second term represents the regularisation term weighted by the parameter λ. The constraint matrix **L** provides the amplitude of the current estimate of the FOD corresponding to the directions along which that amplitude is below the threshold τ, the convergence is achieved when there is no further change in the matrix **L**. To date in the literature, the CSD remains the most popular method used to reconstruct the crossing fibers in the WM from HARDI data with at least 60 DW acquisitions. In 2014, the CSD model was extended to the multi-shell DW-MRI data with the *Multi-tissue constrained spherical deconvolution* method [32].

An alternative representation using Cartesian tensors (CT) [15] imposes elegantly the positivity constraint on the FOD function. The diffusion signal S is thus, a result of a convolution operation between a Cartesian tensor FOD (CT-FOD) F and a Watson function R [15] as follows:

$$S(\mathbf{q}) = \int_{S^2} R(\mathbf{q}, \mathbf{u}_l)F(\mathbf{u})d\mathbf{u} \tag{4}$$

where the integration is over the unit vectors **u**, that uniformly sample the unit sphere, with the parameters **q** corresponding to the gradient of magnetic fields. The Watson function is expressed by $R(\mathbf{q},\mathbf{u}) = e^{-bD(\mathbf{q}^T\mathbf{u})^2}$, and D is a diffusivity coefficient calculated from a 2nd order tensor of a single fiber response with a high fractional anisotropy (FA > 0.8). In this formulation, the FOD F noted CT-FOD is modelled as a positive definite Cartesian symmetric high order tensor of 3 dimensions and written as follows:

$$F(q) = \sum_{a+b+c=d} C_{a,b,c} q_1^a q_2^b q_3^c \tag{5}$$

with $C_{a,b,c}$ the coefficients of the tensor, and $[q_1,q_2,q_3]$ the components of the gradient vector **q**. The positivity constraint is elegantly imposed by re-parameterizing the homogeneous polynomial $F(\mathbf{q})$ of order d in 3 variables as a sum of squares of polynomials of order $d/2$ according to the Ternary quartics theorem [15].

2.2. Fibers orientations detection

Both of the CSD and CT-FOD models describe the whole spherical FOD function in the SH and tensors basis respectively, and consequently, an additional step is required to recover the individual fibers orientations. Traditionally, this can be performed either by an exhaustive local maxima localisation on the sphere when the FOD is described with SH, or by calculating the Z-eigenvalues [20,21] of FOD represented with a Cartesian tensor. However, these traditionnal methods are known to be ineffective in terms of angular resolution which highly depends on the order of the FOD. Recently, methods based on tensor decomposition [22-25] were proposed to extract the local maxima of a symmetric high order tensor FOD with better angular resolution. In the following, we present the concept of tensor decomposition applied to the fibers orientations detection issue. Besides, the tensor decomposition formulation constitutes the base of our spFOD model.

2.2.1. Symmetric tensor decomposition

High order tensors decomposition is a mathematic tool that extracts the geometric and the invariance properties of tensors. The tensor decomposition problem consists in writing a given d-ordered tensor, in a sum of outer product of vectors i.e. rank-1 tensors, with a minimal number of terms:

$$\mathcal{T}^{(d)} = \sum_{i=1}^{r} \lambda_i \mathbf{c}_i^1 \otimes \mathbf{c}_i^2 \otimes \ldots \otimes \mathbf{c}_i^d = \sum_{i=1}^{r} \lambda \mathbf{c}_i^{\otimes d} \tag{6}$$

r being the minimal tensor rank, $C_i = \lambda_i \mathbf{c}_i^{\otimes d}$ rank-1 tensors weighted by λ_i and $(\otimes)$ the outer product operation. In diffusion MRI, the decomposition of a Cartesian symmetric diffusion tensors CT-FOD allows extracting in each voxel, the orientations of WM crossing fibers; in this case, the minimal tensor rank r corresponds to the number of underlying fibers, and the rank-1 tensors correspond to the fibers orientations. However, determining the minimal rank of high order tensors is known to be a hard mathematical and NP-complete problem, low-rank approximation methods like CANDECOM/PARAFAC have been proposed [22-24] to approximate the decomposition of high order tensors with a sub-generic rank $k < r$, where k doesn't exceed 3 [22-24]. In DW-MRI, setting the sub-generic rank k is equivalent to know a priori the number of underlying fibers, which is obviously impossible. Recently, Megherbi et al. [25] proposed an analytical method known as Adecomp-SHOT to recover the fibers orientations by decomposing analytically a high order tensor without any prior information about the tensor rank. The Adecomp-SHOT method exploits the Henkel matrix and the multiplication matrix properties to provide a minimal decomposition with a minimal rank automatically [25].

Finally, all these fibers orientations extraction approaches consider the fibers orientations as oriented delta functions without directly representing them. In the following section we show how to physically model the Dirac delta functions as high order rank-1 tensors, and we propose a novel formulation where the FOD is initially modelled as a sum of high orders rank-1 tensors. The fibers orientations and the FOD are then recovered simultaneously from a non-negative sparse recovery scheme. This new modelisation presents many advantages: the

estimated FOD are non-negatives, the FODs and the fibers orientations are rendered in one step, the number of crossing fibers is rendered automatically, and the most important, FODs of any order can be estimated from limited number of acquisitions allowing acute angular resolution by using few number of DW acquisitions.

2.3. FOD from non-negative sparse recovery: spFOD

Our spFOD [28,33] model is based on the spherical deconvolution operation combined with high order tensor decomposition. Thus, instead of describing the global FOD with tensors or SHs like in CSD or CT-FOD methods, we model individually each oriented Dirac delta function as a rank-1 tensor of order $2n$ as follows:

$$C = \lambda \mathbf{c}^{\otimes(2n)} \tag{7}$$

The FOD tensor described as an unknown r sum of oriented Delta function is given by the following equation, analog to the Eq. (6):

$$\mathcal{F} = \sum_{i=1}^{r} \lambda_i \mathbf{c}_i^{\otimes(2n)} \tag{8}$$

Along an orientation c, the delta function is described by

$$\begin{aligned} C_n(\mathbf{u}) &= \mu_{j_1 j_2 j_3 \ldots j_2 n} C_{j_1 j_2 j_3 \ldots j_2 n} u_{j_1 j_2 j_3 \ldots j_2 n} \\ &= C^{\cdot(2n)} \cdot \mathbf{u} \end{aligned} \tag{9}$$

with $\mathbf{u} \in S^2$ and μ the multiplicity of the coefficients of the $2n$-ordered symmetric rank-1 tensor, the FOD function is then written as:

$$F_n(\mathbf{u}) = \mathcal{F}^{\cdot(2n)} \cdot \mathbf{u} \tag{10}$$

Modelling the FOD with an r-sum of rank-1 tensors or modelling the delta function with rank-1 tensor is justified in Fig. 2. This figure shows rank-1 tensors weighted by ($\lambda = 1$) of increasing order ($2n = 16,24$) and delta function in a truncated SH series (orders 8,12). We notice, that although the SH delta grows rapidly sharper and longer for larger truncation orders, oscillations appear. Whereas, the rank-1 tensor is smooth and gets sharper for larger orders, with λ regulating its length. Besides, in our modelisation since we always estimate three dimensional vectors representing the fiber orientations, the tensor order can be chosen arbitrarily big without increasing the number of unknowns; which allows us to get a highly smooth and sharp rank-1 tensor.

Thus, in our formulation the unknowns are the weights λ_i that cannot be negative, the fibers orientations $\mathbf{c}_i$ and their number r representing the rank of the FOD tensor, $\mathcal{F}$. In the following, we pose the spherical deconvolution problem and we show how to estimate the spFOD function from a diffusion raw signal via a non-negative sparse recovery scheme.

2.3.1. Estimating the spFOD function from a diffusion raw signal

The FOD function is estimated by spherical deconvolution. The original convolution integral of Eq. (1) is discretized to:

$$S(\mathbf{q}_j) = \sum_{l=1}^{L} R(\mathbf{q}_j, \mathbf{u}_l) F(\mathbf{u}_l) \Delta\mathbf{u} \tag{11}$$

The response function $R(\mathbf{q},\mathbf{u})$ is a Watson function that we estimate from single fibers voxels with high fractional anisotropy (FA $>$ 0.8). The function FOD F being an r-sum of rank-1 tensors of even order $2n$ Eq. (10), the previous equation becomes:

$$S(\mathbf{q}_j) = \sum_{i=1}^{r} \lambda_i \sum_{l=1}^{L} R(\mathbf{q}_j, \mathbf{u}_l) \mathbf{c}_i^{2n} \cdot \mathbf{u}_l \Delta\mathbf{u} \tag{12}$$

As noted before, the tensor order ($2n$) can be chosen arbitrarily big without increasing the number of unknowns. However, in practice this may not fit the signal well, so we propose to estimate the tensor order automatically from the data. Since the single fiber signal is given by the convolution between the response function and the single Delta spike and it should be exactly the same as the response function as described in Eq. (13), with the Delta spike oriented along the z-axis.

$$S_z(\mathbf{q}) = R_z(\mathbf{q}, \mathbf{u}) * \underset{C_n(\mathbf{u})}{\delta_z} = R_z(\mathbf{q}, \mathbf{u}) \tag{13}$$

The tensor order can be estimated from voxels with single fiber profile (FA $>$ 0.8) by minimising the following non-linear objective function for (n):

$$\min_n \| S_z(\mathbf{q}) - R_z(\mathbf{q}, \mathbf{u}) * C_n(\mathbf{u}) \|^2 \tag{14}$$

From Eq. (12), we can compute the following minimisation problem for the unknowns X:

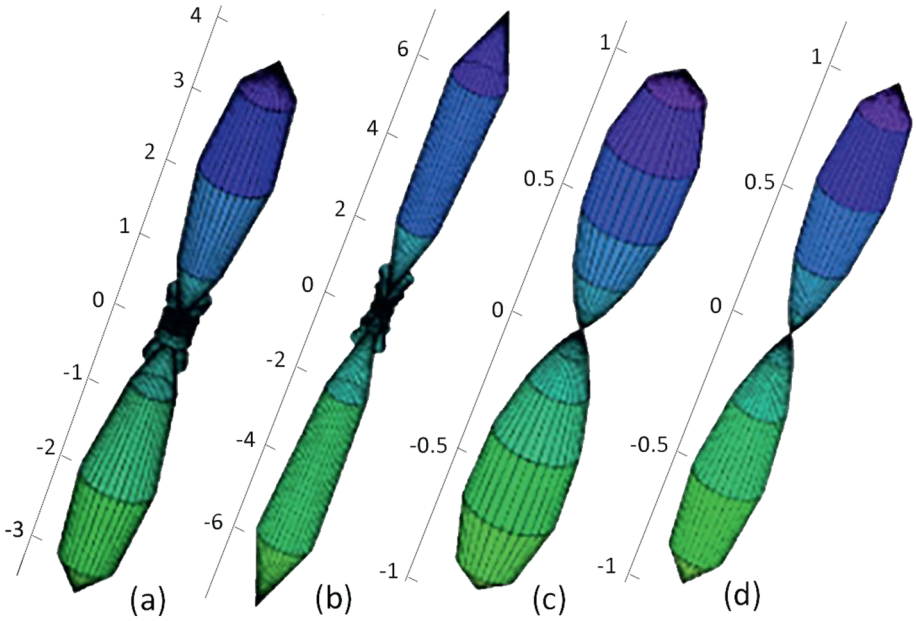

Fig. 2. Delta in SHs: (a) order 8, (b) order 12. Delta as rank-1 tensor: (c) order 16, (d) order 24.

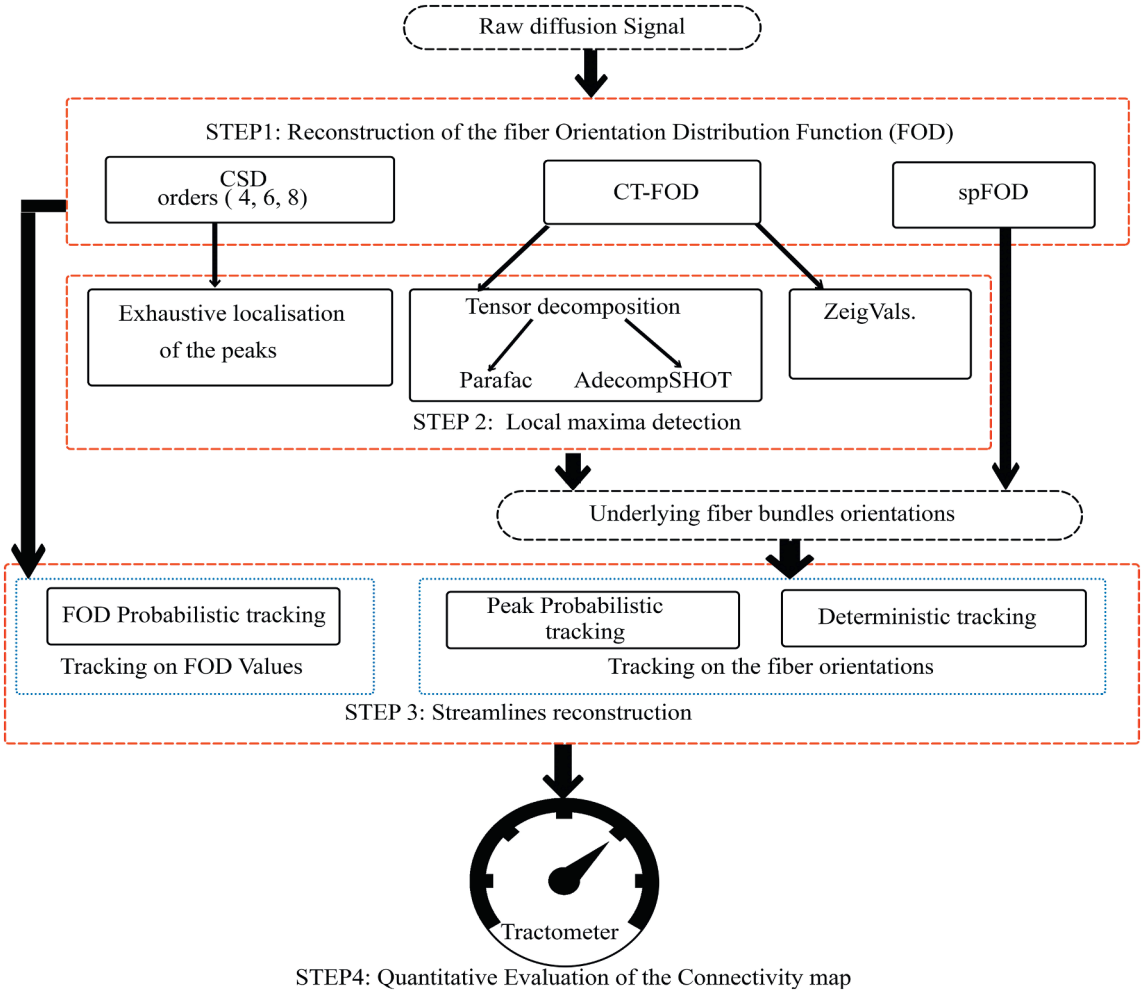

Fig. 3. Scheme of the quantitative analysis of the global connectivity on a simulated DW-MRI data using the tractometer tool: Evaluation and comparison of a set of fiber orientations reconstruction methods. Step 1: reconstruction of the fiber orientation distribution function using the CSD, the CT-FOD and the spFOD methods. Step 2: fibers orientations extraction using an exhaustive localization on CSD, the Z-eigenvalues and tensors decomposition methods on CT-FOD, not necessary for our spFOD method. Step 3: reconstruction of the global connectivity using the probabilistic tracking on the FOD values resulting from step 1, the probabilistic and deterministic tracking on the fibers orientations resulting from step 2 and directly from step 1 for our spFOD method.

Fig. 4. Simulated DW-MRI dataset presenting 27 bundles with complex configurations and crossings angles.

$$\min_{\{X\}} \|\mathbf{Bw} - \mathbf{s}\|^2 \quad st. \quad \mathbf{w} \geq 0, \tag{15}$$

where $\mathbf{s}_j = S(q_j)$, $\mathbf{w}_i = \lambda_i$ and $\mathbf{B}_{ij} = \sum_{l=1}^{L} R(\mathbf{q}_j, \mathbf{u}_l)\mathbf{c}_i^{2n}$. $\mathbf{u}_l\Delta\mathbf{u}$, with L representing the discretization of the convolution. In the low-rank approximation methods of the literature [22-24], the rank r been fixed a priori to a value ($k < r$), the unknowns are $\{X\} = \{\lambda_i, \mathbf{c}_i\}$. In our resolution method, the rank r is not fixed, we consider in the beginning a large set of vectors $\{\tilde{\mathbf{c}}\}$ from a fine discretization of S^2, thus, we take an initial set of 321 vectors isotropically distributed on a hemisphere, according to the work of Jian et al. [11]. Thus, for these initial set of vectors or rank-tensors we let the initial FOD $\tilde{\mathcal{F}} = \sum_{i=1}^{\tilde{r}} \lambda_i \tilde{\mathbf{c}}_i^{\otimes 2n}$ with initial rank $\tilde{r} = 321$, the unknowns are then $\{X\} = \{\lambda_i\}$.

Since very few crossing fibers are expected in a voxel, we estimate the weights $\mathbf{w} = \{\lambda_i\} \geq 0$ from Eq. (15) with a sparsity constraint. One could think of using the L_1/L_0 regularisation, however, Jian et al. [11] have compared L_1/L_0 regularisation with the NNLS algorithm [34] for application to spherical deconvolution techniques in dMRI, and showed that L_1/L_0 do not typically respect the non-negativity constraint and even in terms of sparse recovery, NNLS finds not only a non-negative solution but also a solution considerably more sparse than L_1/L_0 [11,33]. For that, we chose to employ the NNLS algorithm to estimate the non-negative weights $\mathbf{w}$ [11,15,33]. To account for noise, we apply a heuristic cleaning on the NNLS results, which consists to remove any $\lambda_i < 0.1.\ \lambda_{\max}$ and merge $\tilde{\mathbf{c}}_i$ & $\tilde{\mathbf{c}}_j$ if $\text{ang}(\tilde{\mathbf{c}}_i, \tilde{\mathbf{c}}_j) \leq 15°$, by calculating the normalized sum of the three dimensional vectors $(\tilde{\mathbf{c}}_i, \tilde{\mathbf{c}}_j)$. The remaining number of non-zero λ_i is considered as the "true rank" $\hat{r}$, of $\mathcal{F}$.

With the tensor order ($2n$) and the known minimal rank $\hat{r}$, we refit the signal by considering the remainders λ_i and their corresponding $\tilde{\mathbf{c}}_i$ estimated in the previous step, as starting solutions of the following optimization problem (Eq. (16)). This minimisation problem (Eq. (16))

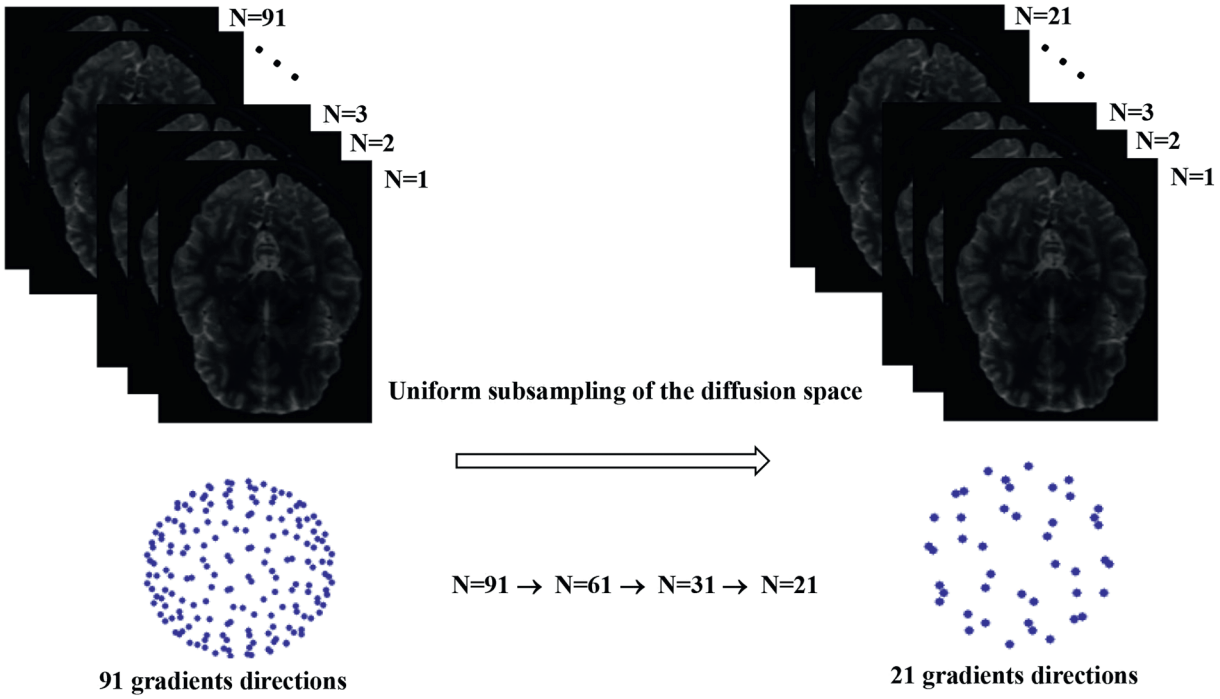

Fig. 5. In vivo DW-MRI data: Uniform sub-sampling of the diffusion space, generating subsets data of 61, 31 and 21 directions from the HARDI HCP data of 91 directions.

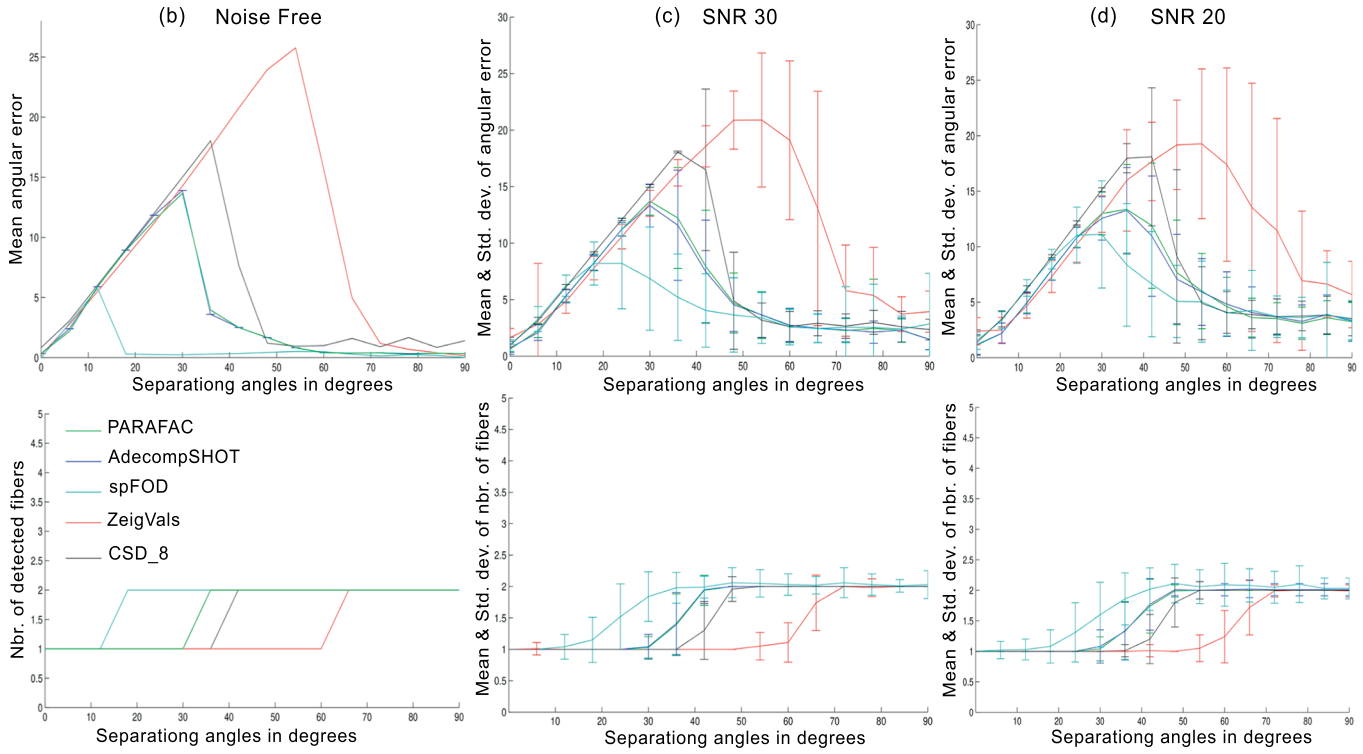

Fig. 6. Synthetic multi-tensors data of 60 gradient directions: (a, b, c) noise free, SNR 30 and SNR 20 respectively. (a, b, c)-superior row: the mean and the standard deviation of the mean error in degrees according to the separating angles. (a, b, c)-inferior row: the mean and the standard deviation of the number of detected fibers according to the separating angles. (For interpretation of the references to color in this figure, the reader is referred to the web version of this article.)

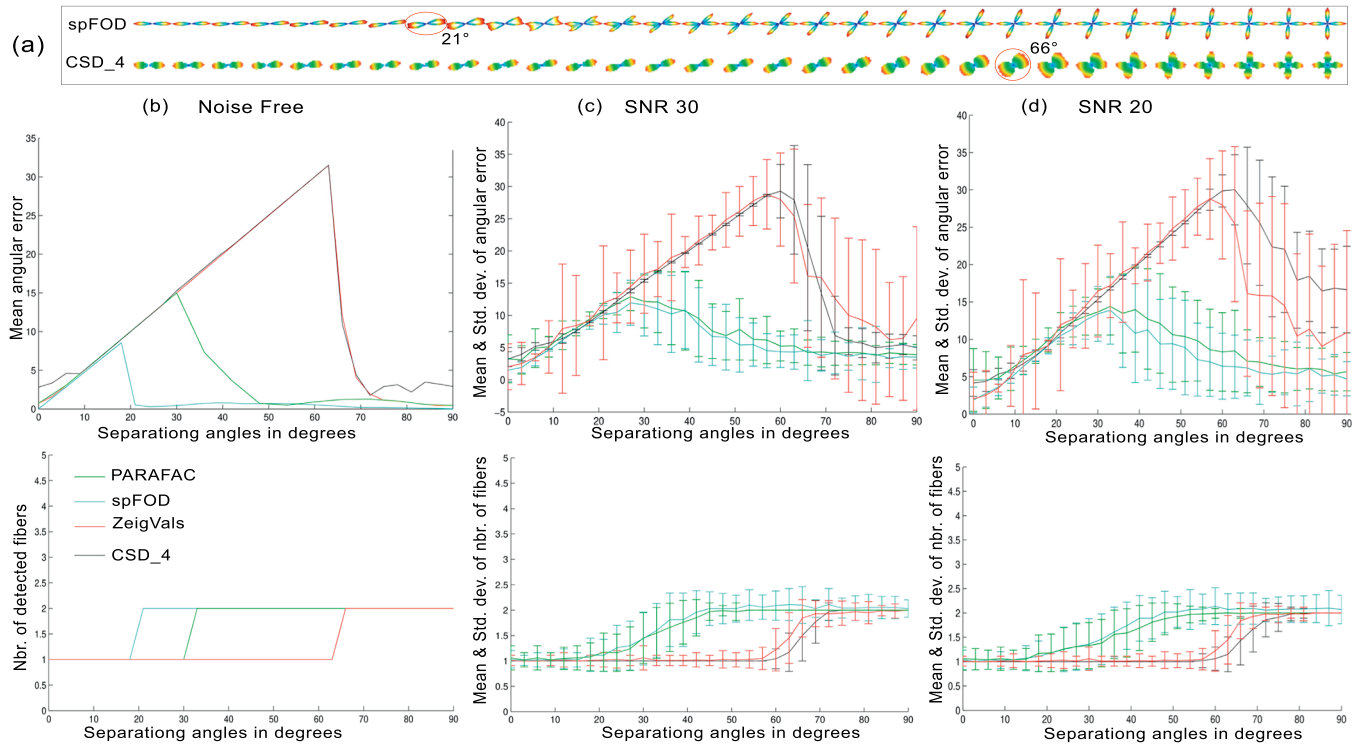

Fig. 7. Synthetic multi-tensors data: (a) FOD tensors as spherical functions. (b) noise free with 21 acquisitions, (c–d) SNR 30 and SNR 20 with 32 gradient directions, respectively. (b, c, d)-superior row: the mean and the standard deviation of the mean error in degrees according to the separating angles. (b, c, d)-inferior row: the mean and the standard deviation of the number of detected fibers according to the separating angles.

re-estimates both the shape of the FOD and fine tuned non-negatives solutions $\widehat{\lambda_i}$, $\widehat{\mathbf{c}_i}$ that fit the signal well.

$$\min_{\{\widehat{\lambda_i},\widehat{\mathbf{c}_i}\}}(\|S(\mathbf{q}_j) - \sum_{i=1}^{\hat{r}} \widehat{\lambda_i} \sum_{l=1}^{L} R(\mathbf{q}_j, \mathbf{u}_l)\widehat{\mathbf{c}_i}^{2n}.\ \mathbf{u}_l\Delta\mathbf{u}\|^2 \tag{16}$$

In the following, we present our validation experiments and results, where we introduce our validation methodology used to evaluate the performance of the spFOD method on the base of the global resulted connectivity. For that, we employ different types of data [35,36], different tractography algorithms [37-39] for the global connectivity reconstruction and we use the tractometer tool [29] to analyze quantitatively the resulted connectivity. Furthermore, to compare our spFOD method to the literature we also evaluate different other methods with the same validation pipeline.

3. Validation experiments

We propose here a scheme to evaluate the performance of our spFOD model not only locally, but also for the global connectivity reconstruction comparing it to the CSD. Our method is also compared to the CT-FOD model combined with different maxima extraction methods as the Z-eigenvalues, PARAFAC and the Adecomp-SHOT. Thus, like illustrated in the methodology scheme (Fig. 3), we quantify on simulated DW-MRI data [35], with known ground truth, the impact of the fibers orientations extraction and the FOD reconstruction on the global connectivity resulted from deterministic tractography [37], probabilistic tractography on the fibers orientations (peak-probab algorithm) [37] and probabilistic tractography directly on the FOD values (fod-probab algorithm) [37].

We begin by testing the voxelwise angular resolution and accuracy of the fiber bundle orientations detection. We then analyze the tractography result with the tractometer tool [29], which is able to quantify the validity of the reconstructed streamlines using the various modelling methods.

Finally, we evaluate qualitatively the performance of our spFOD method in extracting the crossing neuronal fibers from in vivo DW-MRI data, when we reduce the number of acquisitions (gradient directions) from 91 to 21. In the remainder, we will refer to the number of DW-MRI acquisitions by the number of gradient directions.

3.1. Validation tools

3.1.1. Data

3.1.1.1. Synthetic multi-tensor diffusion data. To evaluate the local angular resolution and accuracy of our spFOD method in detecting crossing fibers, we use the multi-tensor model to generate synthetic datasets of 60 and 21 gradient directions with *b*-values of 3000 s/mm^2 and 1500 s/mm^2 respectively, representing crossing fibers with variable separating angles from 90° to 0°. Then, we corrupt datasets of 60 and 32 gradient directions with Rician noise of SNR 20 and 30, to study the effect of noise. For each SNR level and separating angles, 100 trials of noise were performed.

3.1.1.2. Simulated DW-MRI data. We use in the quantitative validation a simulated DW-MRI dataset (Fig. 4) proposed in the IEEE International Symposium on Biomedical Imaging (ISBI) 2013 Reconstruction Challenge [35,40]. This data consists of 27 fibers bundles with a wide range of configurations: branching, kissing and crossing fibers at angles varying from 30° to 90°. For our study, we use two types of acquisitions,

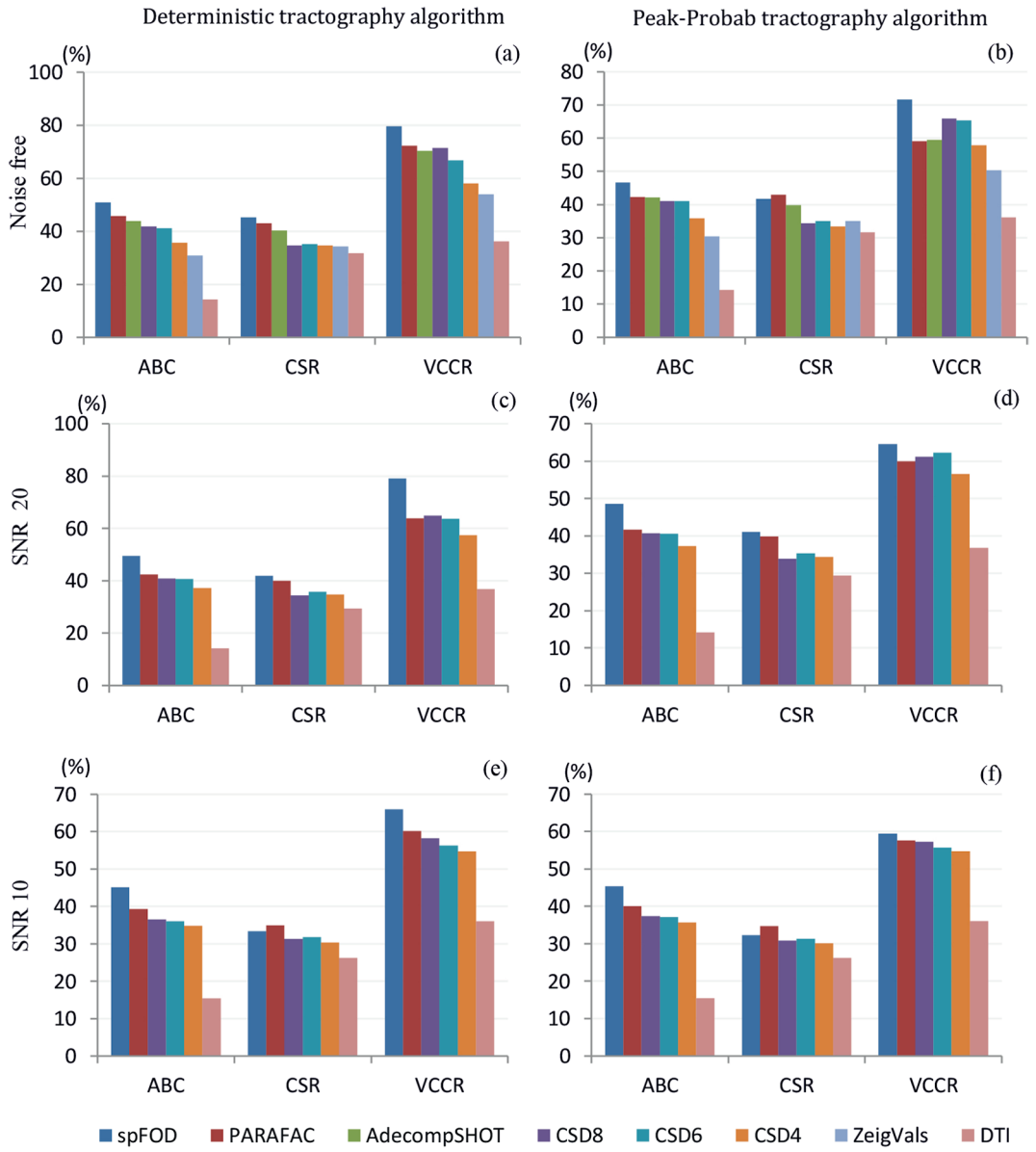

Fig. 8. Diffusion data of 60 gradient directions: Tractometer parameters (ABC, CSR, VCCR) obtained from deterministic and peak-probab tracking based on different fiber orientations extraction methods. (a-c-e) The results with a deterministic tractography, (b-d-f) Results with peak-probab tractography. Superior row: noise free data. Middle row: noisy data with Rician noise of SNR 20. Inferior row: Noisy data with Rician noise of SNR 10.

the HARDI acquisition with 60 gradient directions weighted with a *b*-value of $b = 3000\,s/mm^2$ and low angular resolution acquisition with 30 gradient directions weighted with a $b = 1200\,s/mm^2$. We corrupt each of them with a signal Rician noise ratio of 20 and 10. Knowing the ground truth connections allows us to quantify the connectivity obtained with different evaluated methods, using the tractometer tool [29].

3.1.1.3. In vivo DW-MRI data. We use the Human Connectome Project data [36] to conduct our in vivo DW-MRI data analysis. Thus, for the qualitative comparison between HARDI data results and the ones obtained with a few number of gradient directions, we use datasets of 91, 61, 31 and 21 gradient directions. However, to avoid the registration operation biases between the different data, we consider an initial public HCP multi-shell data of 91 gradient directions [41] then, we select one shell of $b = 1000\,s/mm^2$ and we generate subsets data of 61, 31 and 21 gradient directions by sub-sampling uniformly the diffusion space (Fig. 5) using the sampling scheme proposed by Caruyer et al. in Ref. [41].

3.1.2. The tractometer

The tractometer [24] is a validation tool that allows analyzing quantitatively streamlines resulted from tractography algorithms. The tractometer renders metrics quantifying the reliability and the accuracy of the connections of the tractography algorithm. Thus, in our work we measured from the tractometer the following parameters: Valid Connections (VC), Invalid Connections (IC), No Connections (NC), Connections to Seed Ratio (CSR), Valid Connections to Connections Ratio (VCCR), the Average Bundle Coverage (ABC), Valid Bundles (VB) and Invalid Bundles (IB); the definitions of these metrics are given in Appendix A.

3.1.3. Tractography algorithms

To evaluate pertinently the different fibers orientations extraction methods and their impact on the tractography results, we use an in-house deterministic and probabilistic tractography algorithms as

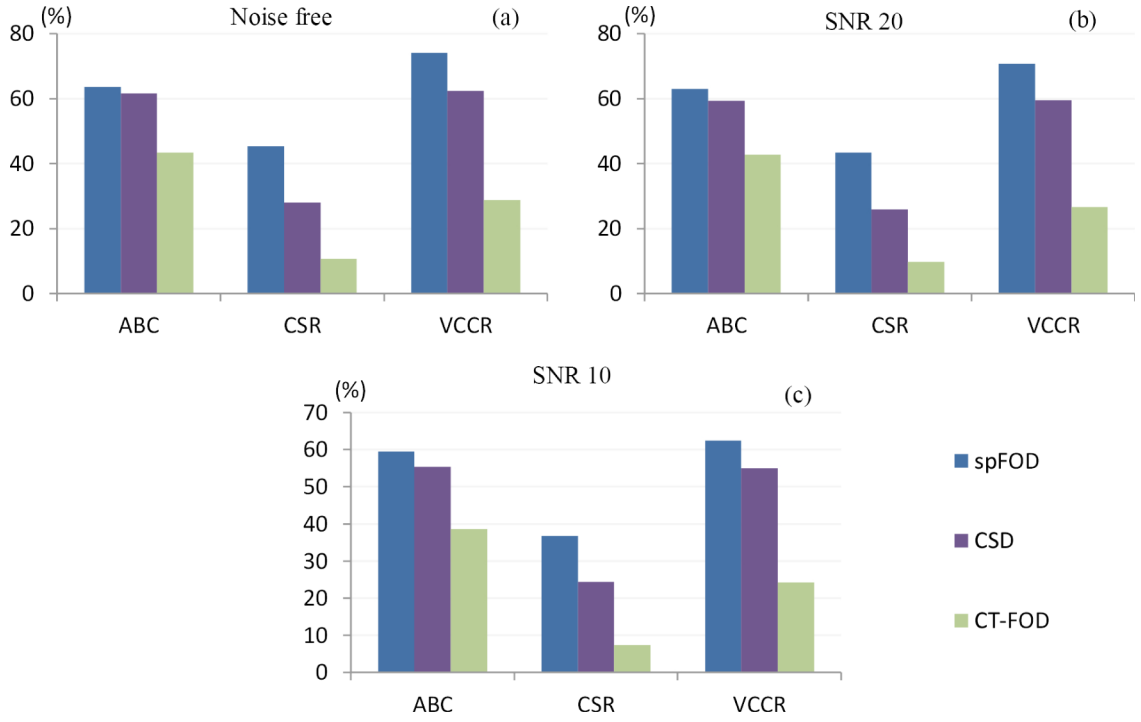

Fig. 9. Diffusion data of 60 gradient directions: Tractometer parameters (ABC, CSR, VCCR) in percentage obtained from FOD probabilistic tracking based on different FOD reconstruction methods. (a): noise free data. (b): noisy data with Rician noise of SNR 20. (c): Noisy data with Rician noise of SNR 10.

Table 1
Valid Bundles (VB) and Invalid Bundles (IB) counts using 60 and 30 gradient directions.

Metric	Number of gradient directions	Tractography	Method	Noise free	SNR 20	SNR 10
VB	60	Deterministic	spFOD	27	27	27
			PARAFAC	26	27	26
			CSD	26	25	25
		Probabilistic	spFOD	26	27	26
			PARAFAC	26	27	26
			CSD	26	25	25
	30	Deterministic	spFOD	27	26	26
			PARAFAC	25	27	25
			CSD	23	23	22
		Probabilistic	spFOD	27	27	27
			PARAFAC	24	26	25
			CSD	23	23	22
IB	60	Deterministic	spFOD	36	42	61
			PARAFAC	28	40	55
			CSD	32	41	54
		Probabilistic	spFOD	37	50	82
			PARAFAC	34	45	58
			CSD	35	43	69
	30	Deterministic	spFOD	32	71	107
			PARAFAC	20	60	96
			CSD	48	65	74
		Probabilistic	spFOD	25	100	142
			PARAFAC	36	70	106
			CSD	51	63	75

described in [37]. The fod-probab algorithm samples directions of the FOD in a maximum angle of 20° from the previous direction with a step size of 0.2 mm [37-39]. The deterministic algorithm follows the peak of the FOD that has the minimum angle with the previous direction and within a maximum angle of 45°, with a step size of 0.5 mm [37]. We also extend the deterministic algorithm to not solely follow the peaks minimising the angle between consecutive tracking steps but to allow the propagation to any of the peaks in a maximum opening angle of 45°, this variant is noted peak-probab algorithm. For all reconstructions, tractography was initiated from all voxels of the white matter mask (in vivo data: 1 seed/voxel, simulated data: 10 seeds/voxel).

3.2. Results and discussion

3.2.1. Quantitative analysis at a voxel: local angular resolution and accuracy

Fig. 6 illustrates the angular resolution and accuracy of different crossing fibers detecting methods evaluated on a synthetic dataset of 60 gradient directions. In the superior row of Fig. 6, we plot the mean and standard deviation of the mean error between the two recovered fiber orientations and the ground-truth orientations. The mean and standard deviation of the number of recovered fibers are represented on the inferior row of Fig. 6. From Fig. 6 a, we clearly notice that the local performance separates the evaluated methods into three groups. In fact, with 60 gradient directions, our spFOD method outperforms all the other methods by detecting the two crossing fibers with an angular resolution limit of 12°. Moreover, the detection error up to 18° is under 1°, indicating the high accuracy of the method (Fig. 6 a, cyan-line). Using 60 gradient directions, both tensor-decomposition based approaches (Fig. 6 a, blue and green-lines) applied on a fourth order CT-FOD function recover the two crossing fibers separated with angles superior to 30°, with a detection error not exceeding 4°, up to a crossing angle of 36°. The exhaustive localisation method used to extract the peaks of the CSD function of spherical harmonics of order 8 allows to recover the two crossing fibers at angles superior than 39° with a detection error under 4° up to a crossing angle of 48° (Fig. 6 a, black-line). The eigenvalues based approach applied on the fourth order CT-FOD is the least efficient method with an angular resolution limit of 60° (Fig. 6 a, red-line).

The effect of a Rician noise: In order to evaluate the effect of noise, we conduct experiments with the same synthetic data of 60 gradient directions corrupted with Rician noise. Fig. 6(b–c) shows the results of 100 tests with SNR = 30 and SNR = 20 respectively. From these figures, we notice the same behaviour than the noise free case where the

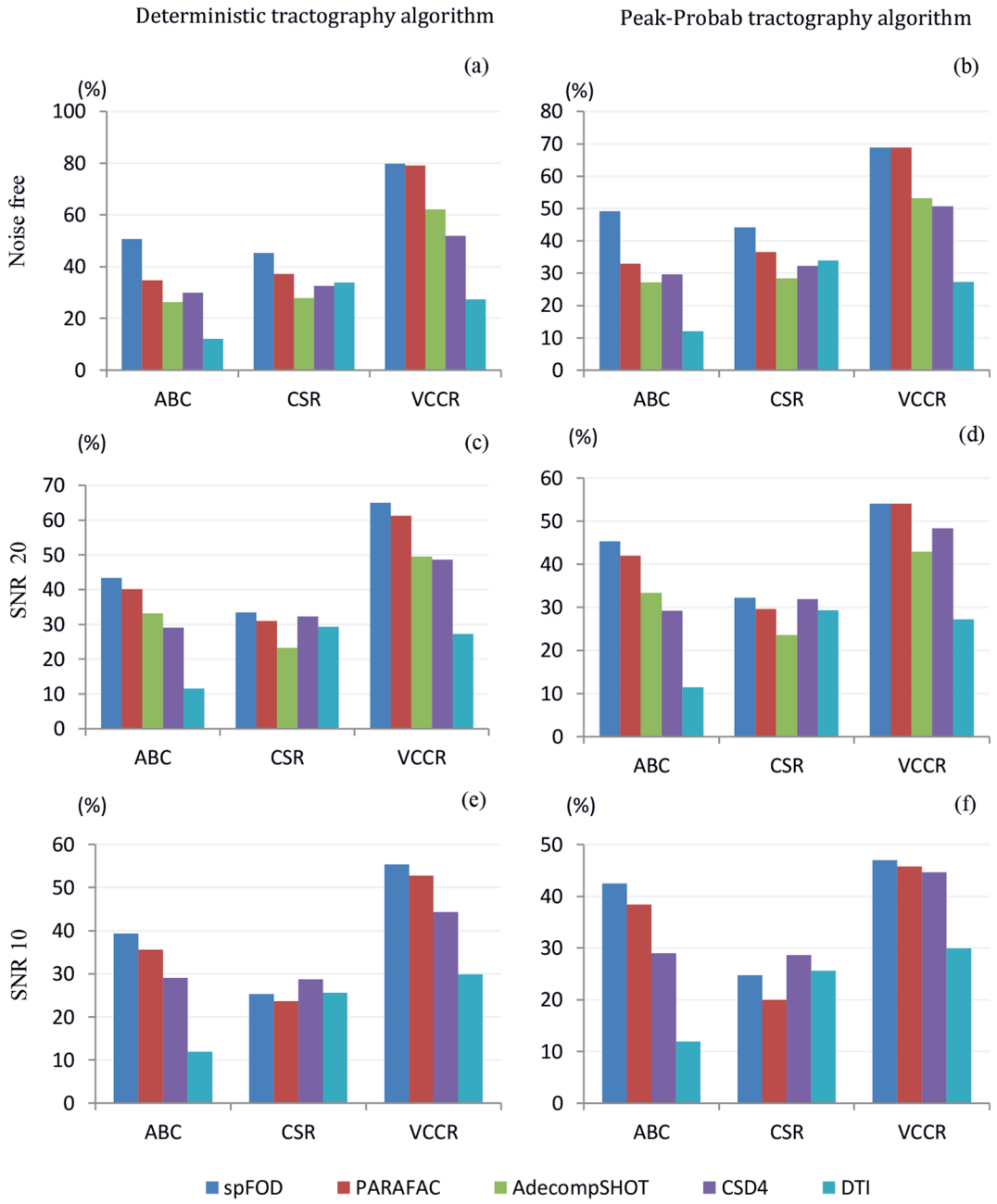

Fig. 10. Diffusion data of 30 gradient directions: Tractometer parameters (ABC, CSR, VCCR) obtained from deterministic and peak-probab tracking based on different fiber orientations extraction methods. (a-c-e) The results with a deterministic tractography, (b-d-f) Results with peak probabilistic tractography. Superior row: noise free data. Middle row: noisy data with Rician noise of SNR 20. Inferior row: Noisy data with Rician noise of SNR 10.

spFOD method remains the most efficient with an angular resolution limit of 18° and 21° for SNR 30 and 20, respectively. For instance, in case of SNR = 30, the two crossing fibers are detected with a mean angular error not exceeding 6° up to a separating angle of 36°. The tensor decomposition methods applied on the CT-FOD and the exhaustive localisation of the CSD's peaks give a similar performance with an angular resolution limit between 30° and 36°, and a detecting error not exceeding 5° up to a separating angle of 48°. The Z-eigenvalues method remains the least efficient with an angular resolution limit of 60° and for a separating angle of 72°, the detecting error is superior to 5° at SNR 30 (10° at SNR 20). Nonetheless, with 60 acquisition DW data, the results indicate good robustness to noise for all the evaluated methods.

Fig. 7a shows the FOD reconstructed with our spFOD method (Fig. 7 a, superior row) and the CSD function (Fig. 7 a, inferior row) from synthetic dataset of 21 gradient directions, representing crossing fibers separated with angles varying from 90° to 0°. We represent these two functions to visualise and compare the spherical profile of our spFOD function to the CSD. Using our sparse recovery scheme, we can reconstruct sharp FODs and discern narrow crossing fibers from a limited number of acquisitions. On this synthetic dataset, we extracted the fiber orientations with different reconstruction methods and evaluate the local angular resolution and error. The results on Fig. 7b show that the spFOD is able to recover the two crossing fiber orientations up to a separating angle of 21° with a detecting error not exceeding 1° from only 21 gradient directions. The PARAFAC tensor decomposition method keeps the same angular resolution limit of 30° as in case of 60 gradient directions, but, this numerical method requires to set a priori the number of underlying crossing fibers. This constitutes an advantage and makes the method sub-optimal in real case where the ground truth

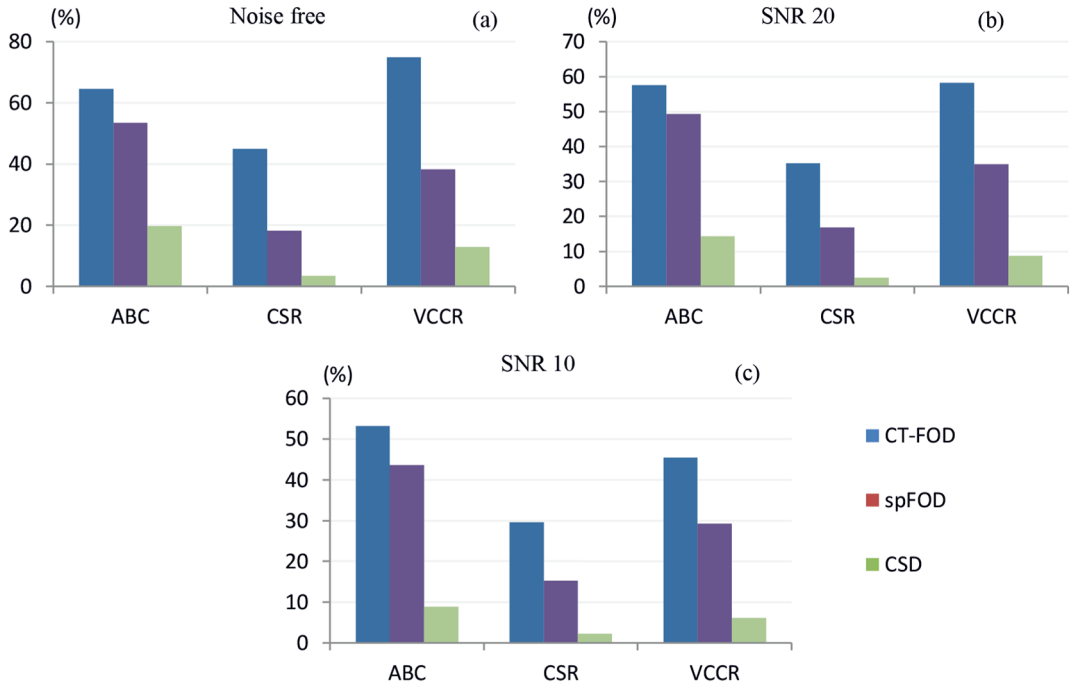

Fig. 11. Diffusion data of 30 gradient directions: Tractometer parameters (ABC, CSR, VCCR) in percentage obtained from FOD probabilistic tracking based on different FOD reconstruction methods. (a): noise free data. (b): noisy data with Rician noise of SNR 20. (c): Noisy data with Rician noise of SNR 10.

is unknown. From only 21 gradient directions, we can estimate CSD with spherical harmonics of order 4 that has an angular resolution limit of 63°, we notice the same performance for the Z-eigenvalues based approach applied on fourth order CT-FOD.

The effect of a Rician noise: Additional experiments were conducted on the noisy synthetic dataset generated using the multi-tensor model with 32 gradient directions. We run 100 tests with SNR = 30 and SNR = 20 for each separating angles that varying from 90° to 0°. Fig. 7(c–d) represents the results with SNR = 30 and SNR = 20 respectively. All the evaluated methods are more sensitive to noise with 21 gradient directions than with 60 gradient directions. The angular resolution limit of our spFOD decreases from 27° to 30° with the decrease in the SNR from 30 to 20. For SNR = 30, the error stays under 6° up to 40°. For SNR = 30, the PARAFAC method seems to have a similar performance than our spFOD approach, with the condition to know a priori the number of crossing fibers in the compartment. The Z-eigenvalues method and CSD using spherical harmonics of order 4 have the highest values of the mean angular error and standard deviation for both SNR = 30 and SNR = 20.

3.2.2. *Quantitative analysis of the streamlines on HARDI simulated data of 60 gradient directions*

In Figs. 8 and 9, we plot the tractometer metrics obtained with 60 DW acquisitions on the simulated DW-MRI dataset using different fibers orientations extraction methods. Fig. 8 illustrates the results for a deterministic tractography and a peak-probab tractography algorithm, in case of noise free data (Fig. 8, superior row), the valid connection to connection ratio (VCCR) indicates three levels of performance for both tractography algorithms. For instance, for the deterministic tractography algorithm, with noise free data, the CSD order 4 (CSD_4) and the Z-eigenvalues of a fourth order CT-FOD have the lowest values with a VCCR not exceeding 58%. As expected, the $CSD_{6,8}$ of higher spherical harmonics orders, PARAFAC and Adecomp-SHOT methods have a higher VCCR varying between 66.8% and 72.2%. The spFOD has a higher VCCR of 79.5%. The same observations are noted with the average bundle coverage ABC and the connection to seed ratio CSR. The graphs of the peak-probab algorithm (Fig. 8, right columns) have a similar trend where the CSD order 4 and the Z-eigenvalues present the lowest values for the metrics VCCR, CSR and ABC, whereas the spFOD presents the highest values for the three last metrics. These results are coherent with the results of Fig. 6, based on the local measurement of the angular resolution and accuracy. In fact, we notice from our first experiment that, the fourth order tensor decomposition methods as PARAFAC or Adecomp-SHOT produce a better global connectivity than the traditionnal methods, as concluded in Refs.[23,25]; we also confirm that the performance of the CSD highly depends on the order of the SH basis.

We illustrate in Fig. 8 (middle and inferior rows) the tractometer metrics for SNR 20 and 10 respectively; we notice that the tensor decomposition and the $CSD_{8,6}$ methods perform similarly. Our spFOD presents slightly higher values of VCCR, CSR and ABC.

Using 60 diffusion data gradient directions (Table 1), the number of valid bundles (VB) is also the highest with spFOD with a score of 27/27 against a maximum of 26/27 for CSD_8. The spFOD and the CSD_8 report a similar number of invalid bundles (IB) varying between 30 and 40 in the noise free case and increasing to 61 for spFOD for SNR 10 (54 for CSD_8 with the same SNR).

3.2.2.1. Evaluation of the fiber orientation distribution reconstruction methods on tractography results. To evaluate the performance of the reconstruction methods CT-FOD, CSD and spFOD, we conduct further tests with the fod-probab tractography algorithm, the results are shown in Fig. 9. All the tractometer metrics ABC, CSR and VCCR, indicate that the spFOD is the most accurate reconstruction method with a higher VCCR of 74.1% in the noise free case and 70.8% for SNR = 20 against 59% for the 8th order CSD and 26.7% for the 8th order CT-FOD. This last one has the lowest VCCR due to its positivity constraint that affects the local angular resolution making the FOD smoother.

As it was explained in the theoretical part (Section 2.3), the particularity and the most important advantage of our spFOD method is its ability to reconstruct correctly multiple crossings fibers with limited number of acquisitions. To validate this performance, we reconduct the tests but now with only 30 gradient directions.

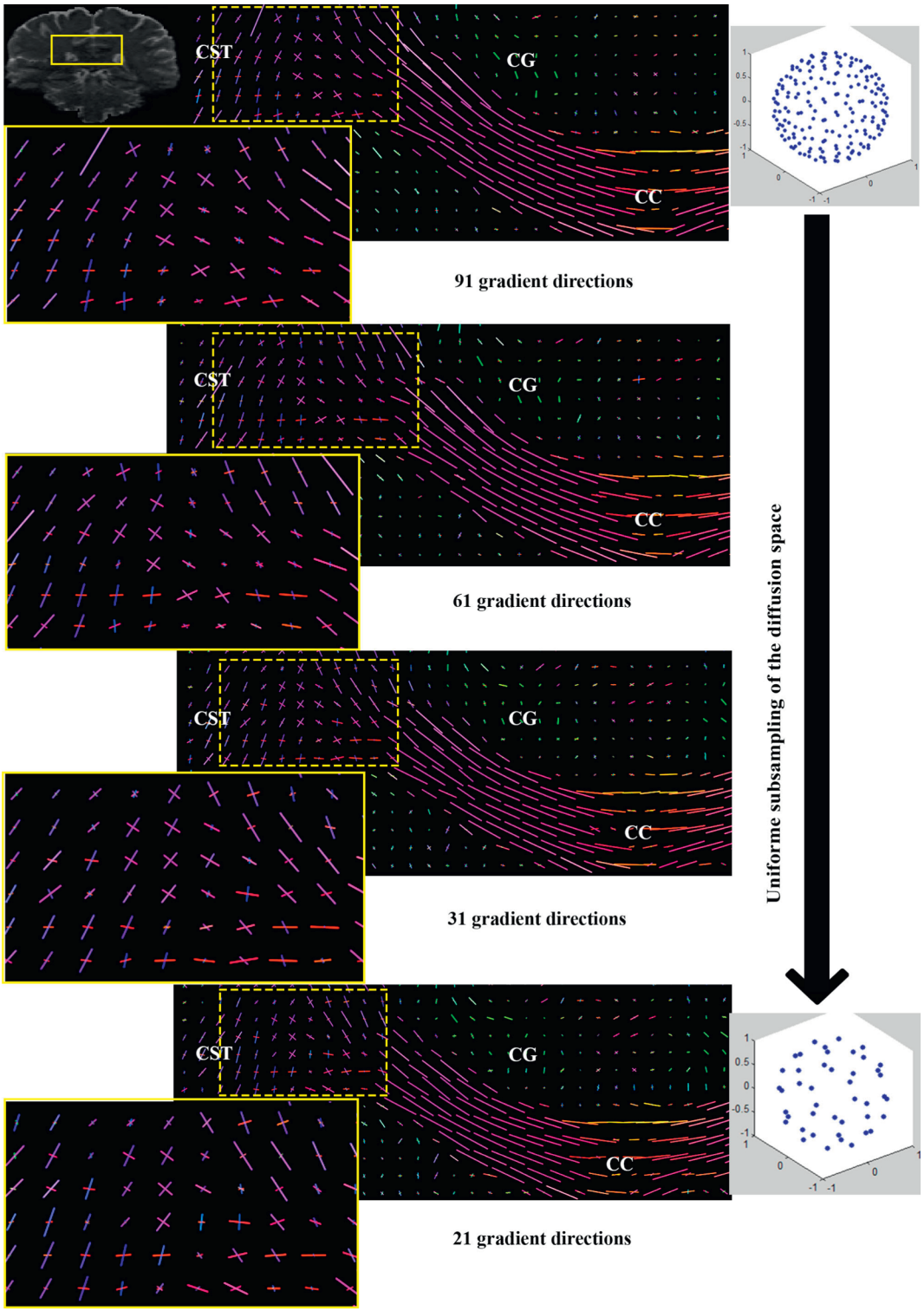

Fig. 12. Fibers orientation extraction on in vivo diffusion DW-MRI data using the FOD from non-negative sparse recovery method: from Top to bottom, the number of gradient directions is reduced from 91 to 21 by a uniform sub-sampling of the same diffusion space. Most crossings of the Corpus Callosum (CC) and the Corticospinal Tract (CST) can be estimated with only 31 and 21 gradient directions.

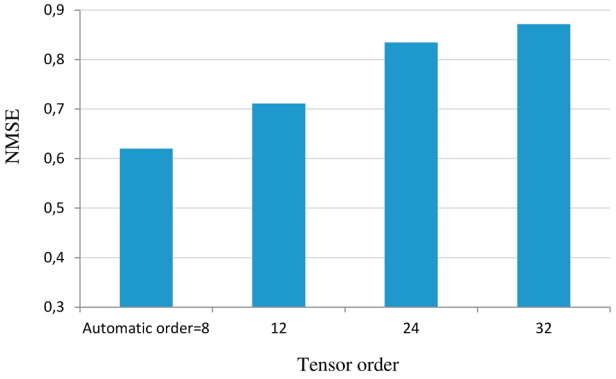

Fig. 13. Normalized Mean Square Error (NMSE) calculated in a ROI of the in vivo dataset, between the original DW-MRI signal and the signals reconstructed from FODs estimated with different orders: 8 (automatic order), 12, 24 and 32.

3.2.3. Quantitative analysis on simulated data of 30 gradient directions

We evaluate all the crossing fiber detection methods that can perform with low number of acquisitions: the PARAFAC and the Adecomp-SHOT methods applied to the CT-FOD of order 4, the CSD of spherical harmonics of order 4 and our spFOD method. The VCCR, CSR and ABC on Fig. 10 show that our spFOD method outperforms the evaluated method with a VCCR of 79.5%. Indeed, even though the numerical PARAFAC approximation method presents good results this must be interpreted carefully because in this method the number of crossing fibers is set a priori to number two, which is surely an advantage since the used simulated DW-MRI data contains many voxels with two fiber crossings. The results on Fig. 10 indicate also that in case of a low number of gradient directions, the Adecomp-SHOT and the CSD_4 have similar performances. Most importantly, we notice from this experiment that for the noise free case, our spFOD model is the only one that provides a connectivity with 30 gradient directions as accurate as the one obtained with HARDI data (Figs. 8– 10, superior row), with a VCCR

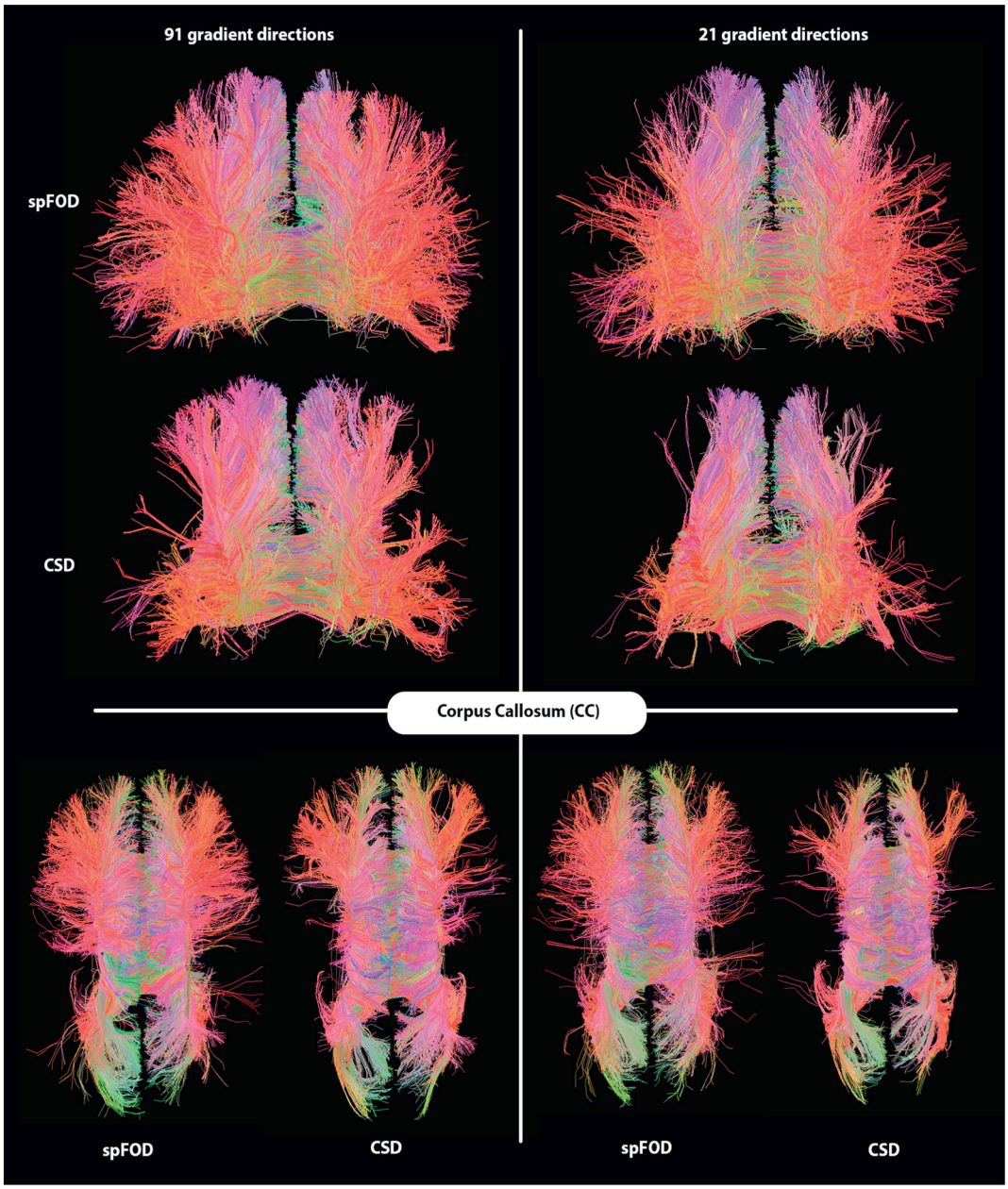

Fig. 14. Corpus Callosum: Reconstruction using deterministic tractography, local fibers orientations extracted using spFOD and CSD from DW-MRI dataset of 91 and 21 gradient directions. (For interpretation of the references to color in this figure, the reader is referred to the web version of this article.)

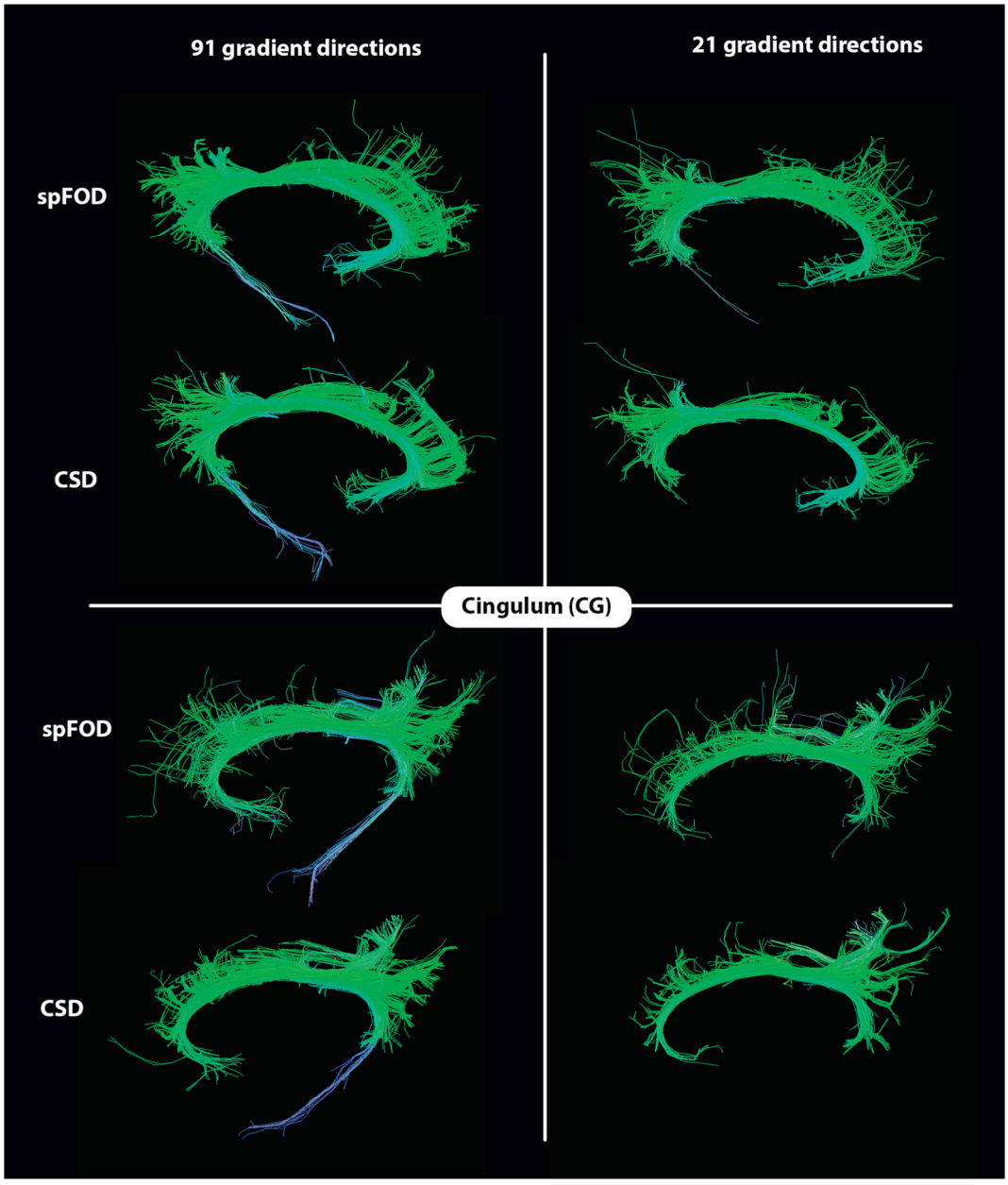

Fig. 15. Cingulum: Reconstruction using deterministic tractography, local fibers orientations extracted using spFOD and CSD from DW-MRI dataset of 91 and 21 gradient directions. (For interpretation of the references to color in this figure, the reader is referred to the web version of this article.)

exceeding 79%, and without requiring any prior information about the fiber orientations. Furthermore, the spFOD is the only method that reports a VB score of 27/27 with a probabilistic tractography (see Table 1), against a maximum of 23/27 for the CSD. In terms of invalid bundles (IB), for both 60 and 30 data acquisitions the best score is reported by the PARAFAC method. This can be explained by the required a priori information on the number of fiber bundles per voxel for this method. We can also observe an increase in invalid bundles produced by CSD with lower spherical harmonics orders.

However, in case of 30 gradient directions the spFOD seems to be more sensitive to noise than with 60 gradient directions. For 60 gradient directions, we notice similar VCCR for both noise free and SNR = 20 with a decrease of 0.4% (− 13.5% for SNR = 10) (Fig. 8). For 30 gradient directions, the VCCR decrease is of 14.8% for SNR = 20 and 24.5% for SNR = 10 (Fig. 10). However, spFOD remains more robust to noise than the CSD. In fact, considering a HARDI data of SNR 20, the CSD_8 produce streamlines with a VCCR = 64.9% using a deterministic tractography (Fig. 8, middle row), whereas for the same SNR 20 and the same tractography algorithm, spFOD provides a similar VCCR = 65% with only 30 gradient directions (Fig. 10).

3.2.3.1. Evaluation of the fiber orientation distribution reconstruction methods on tractography results. The previous results are coherent with those given by Fig. 11. Effectively, plotting the tractometer metrics returned for the fod-probab tractography reveals that for a dataset of only 30 gradient directions our spFOD method provides the similar streamlines as for 60 gradient directions. In fact, spFOD produces the highest valid connection to connections ratio with a VCCR > 74% for noise free data, against 38.2% and 12.9% for the fourth order CSD and CT-FOD respectively (Fig. 11 a). All the methods are more sensitive to noise with 30 gradient directions than 60 gradient directions (Fig. 11 (b–c)).

We conclude from the quantitative analysis of the global connectivity that the spFOD allows us to reconstruct more accurately

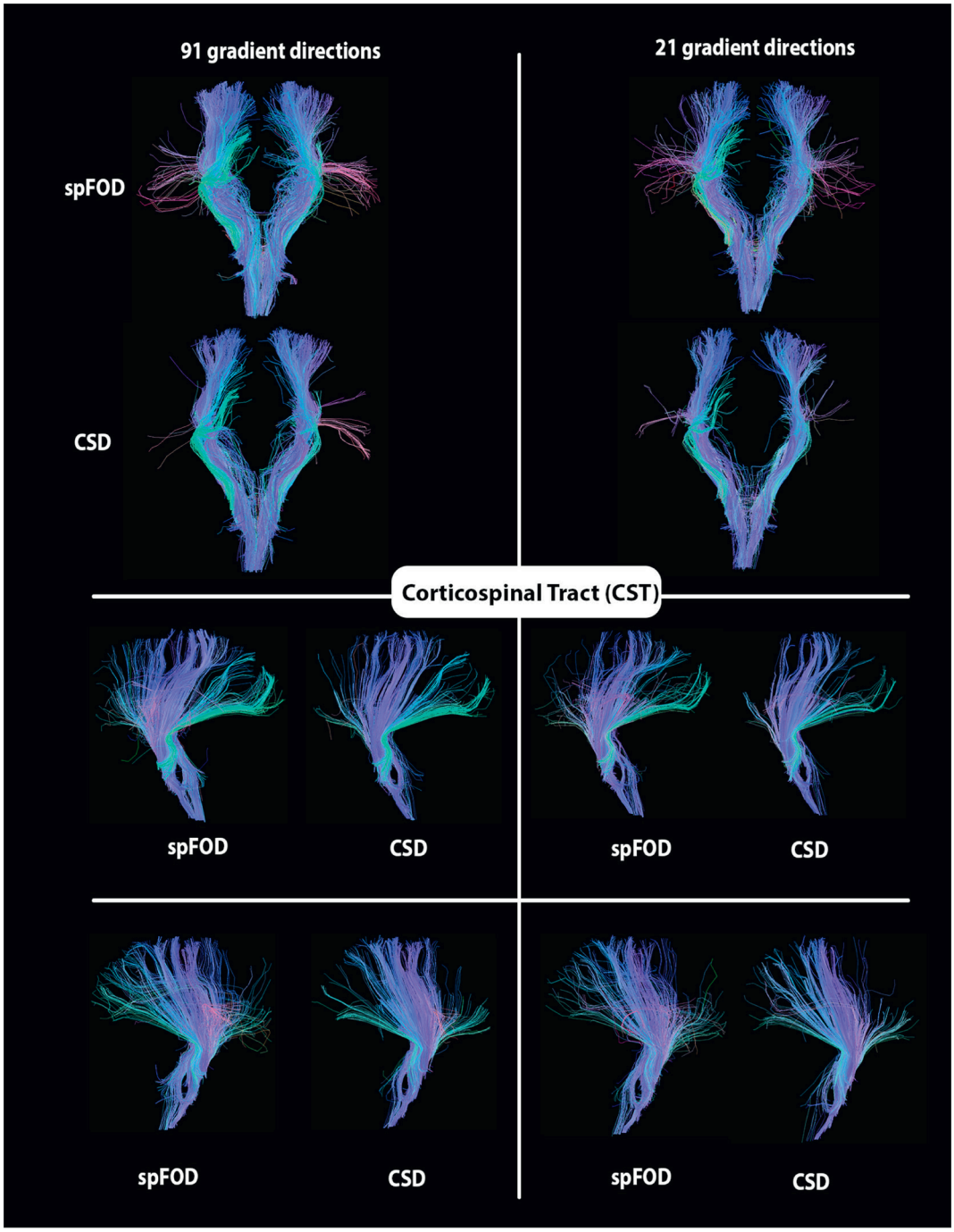

Fig. 16. Corticospinal Tract: Reconstruction using deterministic tractography, local fibers orientations extracted using spFOD and CSD from DW-MRI dataset of 91 and 21 gradient directions. (For interpretation of the references to color in this figure, the reader is referred to the web version of this article.)

streamlines with only 30 gradient directions without requiring any prior information about the number of underlying crossing fibers. In the following, we conduct additional validation tests on in vivo DW-MRI data to show the performance of our spFOD method in extracting the neuronal fiber bundles from in vivo DW-MRI data of 91 to 21 gradient directions.

3.2.4. Evaluation on in vivo DW-MRI data

Fig. 12 illustrates the results of fiber orientations extraction from an in vivo DW-MRI data, which are presented in Section 3.1.1 [36]. We focus on a crossing fibers region where the Corpus Callosum (CC) intersects with the Corticospinal Tract(CST). We tested our method first on data of 91 gradient directions, then we generate sub-datasets of 61, 31 and 21 gradient directions, by a uniform sub-sampling of the diffusion space [41]. From Fig. 12, we notice that the local crossings of the Corpus Callosum (CC) and the Corticospinal Tract (CST) are extracted with only 31 or 21 gradient directions. However, as shown with the synthetic dataset in Section 3.2.3, the method seems to be more sensitive to noise with a low number of DW acquisitions.

We mentioned earlier in the paper that the order of FOD can be chosen arbitrarily big, but, in practice this may not fit the signal well, so we propose to estimate the tensor order automatically from the data. To show the goodness of fit we conduct tests on a ROI of the in vivo DW-MRI data, where we calculate the Normalized Mean Square Error (NMSE) between the original DW-MRI signal and the signal reconstructed from FODs estimated with different high orders. The results

presented in Fig. 13 show that the signal reconstructed from the FOD with the order estimated from the data (order = 8) is more accurate than the results obtained with very high orders (12, 24 or 32).

Figs. 14, 15, and 16 show streamlines of the Corpus Callosum (CC), the Cingulum (CG) and Corticospinal Tract (CST) respectively, resulting from a deterministic tractography based on the local fiber orientations extracted from spFOD function and CSD. For all reconstructions, bundles were manually segmented using identically placed regions of interest (CC: commissural streamlines ending in the cortex, CG: association streamlines passing through the central region of the cingulate cortex, CST: projection streamlines passing through the posterior limb of the internal capsule and ending in the brainstem). Streamlines are colored according to their main orientation. The results with 91 and 21 gradient directions are represented on the left and right columns of Figs. 14, 15, and 16 respectively. The right columns of these figures show that our spFOD method can reconstruct intersecting WM fiber bundles from 21 gradient directions. This is coherent with the results obtained locally and represented on Fig. 12.

From Fig. 14, we notice that the CC is better reconstructed with our spFOD method than with the CSD for both 91 and 21 gradient directions. The CG and CST reconstructions don't show large differences between the spFOD and CSD methods. We notice that more of the CG streamlines reconstructed with 91 gradient directions are also reconstructed with 21 gradient directions with the spFOD method (Fig. 15). However, both reconstructions of the CG using 21 gradient directions miss the streamlines reaching the temporal lobes (shown in blue in Fig. 15). Also, the CST presents more lateral projections using the spFOD method compared to the CSD method (Fig. 16).

Finally, the spFOD produces more streamlines than the CSD reconstruction, which might be due to its higher angular resolution. That suggests that spFOD can extract more of true positive peaks, but also produces more false positive peaks. The qualitative evaluation on a real DW-MRI data consolidates the quantitative analysis on a simulated DW-MRI data.

4. Conclusion

In this work, we presented a novel fiber orientation function (spFOD) that can reliably reconstruct narrow crossing fibers and obtain a high quality tractogram even from a limited number of acquisitions. Using a non-negative sparse recovery scheme, we have shown that our method allows to reliably estimate the positive fiber orientation distribution(FOD) Function together with the number of crossing fibers.

We used the tractometer tool to quantify the results of both deterministic and probabilistic tractography algorithms obtained from the simulated noisy dataset and in vivo DW-MRI datasets with high and low angular resolutions and we demonstrated the performance of our FOD model and its impact on the tractography results.

However, our method is modelling solely the white matter signal. As such, regions with partial volume fraction with cerebrospinal fluid or gray matter could bias the fiber orientations estimation. The addition of other signal compartments will be addressed in future work.

Acknowledgments

The authors wish to thank Emmanuel Caruyer for the sharing of the synthetic dataset used in this work, and the Tractometer team (Jean-Christophe Houde, Marc-Alexandre Côté, Maxime Descoteaux, tractometer.org) for the tractography evaluation tool.

This work has received funding from the European Research Council (ERC) under the Horizon 2020 - Research and Innovation Framework Programme (ERC Advanced Grant agreement No.694665: CoBCoM).

Appendix A. Tractometer connectivity metrics

We present below the description of the tractometer connectivity metrics provided by the tractometer tool [29,37].

- Valid Connections (VC): percentage of streamline connecting expected regions of interest (ROIs) (valid regions) [29].
- Invalid Connections (IC): percentage of streamline connecting unexpected ROIs or streamlines connecting expected ROIs but exiting the expected bundle mask. These streamlines do not correspond to the ground truth [29].
- No Connections (NC): percentage of streamline that do not connect two ROIs. These streamlines stop prematurely due to the stopping criterions of the tractography algorithm for example the angular constraints or mask limits [29].
- Valid Bundles (VB): Number of streamline bundles connecting expected ROIs. The maximum number of VB for the simulated dataset is 27 [29].
- Invalid Bundles (IB): Number of streamline bundles connecting unexpected ROIs [29].
- Average Bundle Coverage (ABC): the average of the number of voxels crossed by streamlines divided by the total number of voxels in the bundle (reported in percentage). This is the average proportion of bundle volumes covered by streamlines [29].
- Connections to Seed Ratio (CSR): the ratio in percentage between the number of estimated connections and the number of seeds used by the tractography algorithm [37]. This parameter quantifies the performance of the tractography algorithm and it is calculated by $CSR = \frac{IC + VC}{s}$, with s the number of seeds.
- Valid Connections to Connections Ratio (VCCR): the ratio in percentage between valid connections and all estimated connections $VCCR = \frac{VC}{VC + IC}$ [37]. These parameters quantify the accuracy of the connectivity.

References

[1] Le Bihan D, Breton E. Imagerie de Diffusion In Vivo par Résonance Magnétique Nucléaire. CR Acad Sci Paris 1985;301(1):1109–12.
[2] Basser P, Mattiello J, Le Bihan D. Estimation of the effective self-diffusion tensor from the NMR spin echo. J Magn Reson 1994;103:247–54.
[3] Northam G B, Liégeois F, Tournier J-D, Croft L J, Johns P N, Chong W K, et al. Interhemispheric temporal lobe connectivity predicts language impairment in adolescents born preterm. Brain J Neurol 2012;135:3781–98.
[4] Baker STE, Lubman D I, Yücel M, Allen N B, Whittle S, Fulcher B D, et al. Developmental changes in brain network hub connectivity in late adolescence. J Neurosci 2015;35(24):9078–87.
[5] Dell'Acqua F, Simmons A, Williams S C R, Catani M. Can spherical deconvolution provide more information than fiber orientations? Hindrance modulated orientational anisotropy, a true-tract specific index to characterize white matter diffusion. Hum Brain Mapp 2013;34(10):2464–83.
[6] Descoteaux M, Angelino E, Fitzgibbons S, Deriche R. Regularized, fast and robust analytical q-ball imaging. Magn Reson Med 2007;58(2):497–510.
[7] Laouchedi M, Megherbi T, Khabatti H, Serrat I, Deriche R, Perlbarg V, et al. Odf maxima computation using hill climbing algorithm. IEEE 11th International Symposium on Biomedical Imaging (ISBI). 2014.
[8] Descoteaux M. De l'estimation locale par imagerie q-ball à la tractographie des croisements de fibres. Centre MOIVRE Département d'Informatique Université de Sherbrooke. vol. 3. 2012. p. 377–98.
[9] Tournier J D, Calamante F, Connelly A. Robust determination of the fiber orientation distribution in diffusion MRI: non-negativity constrained super-resolved spherical deconvolution. Neuroimage 2007;35(4):1459–72.
[10] Cheng J, Deriche R, Jiang T, Shen D, Yap PT. Non-negative spherical deconvolution (NNSD) for estimation of fiber orientation distribution function in single-/multi-shell diffusion MRI. Neuroimage 2014;101:750–64.
[11] Jian B, Vemuri B C. A unified computational framework for de-convolution to reconstruct multiple fibers from diffusion weighted MRI. IEEE Trans Med Imaging 2007;26(11):1464–71.
[12] Dell'Acqua F, Rizzo G, Scifo P, Clarke RA, Scotti G, Fazio F. A model-based deconvolution approach to solve fiber crossing in diffusion-weighted MR imaging 562–472 IEEE Trans Biomed Eng 2007;54(03).
[13] Dell'Acqua F, Scifo P, Rizzo G, Catani M, Simmons A, Scotti G, et al. A modified

damped Richardson-Lucy algorithm to reduce isotropic background effects in spherical deconvolution. Neuroimage 2010;49(02):1446–58.
[14] Landman B A, Bogovic J A, Wan H, El Zahraa ElShahaby F, Bazin P L, Prince J L. Resolution of crossing fibers with constrained compressed sensing using diffusion tensor MRI. Neuroimage 2012;59(03):2175–86.
[15] Weldeselassie T Y, Barmpoutis A, Atkins M S. Symmetric positive semi-definite Cartesian Tensor fiber orientation distributions (CT-FOD). Med Image Anal J 2012;16(6):1121–9.
[16] Daducci A, Van De Ville D, Thiran J-P, Wiaux Y. Sparse regularization for fiber ODF reconstruction: from the suboptimality of *l2* and *l1* priors to *l0*. Med Image Anal 2014;18(06):820–33.
[17] Feng Y, Wu Y, Rathi Y, Westin C F. Sparse deconvolution of higher order tensor for fiber orientation distribution estimation. Artif Intell Med 2015;65(03):229–38.
[18] Ramírez-Manzanares A, Rivera M, Vemuri B C, Carney P, Mareci T. Diffusion basis functions decomposition for estimating white matter intra-voxel fiber geometry. IEEE Trans Med Imaging 2007;26(08):1091–102.
[19] Qi L. Eigenvalues of a real supersymmetric tensor. J Symb Comput 2005;40:1302–24.
[20] Bloy L, Verma R. On computing the underlying fiber directions from the diffusion orientation distribution function. Medical Image Computing and Computer-Assisted Intervention – MICCAI 2008. LNCS, vol. 5241. 2008. p. 1–8.
[21] Ghosh A, Wassermann D, Deriche R. A polynomial approach for maxima extraction and its application to tractography in HARDI. Information Processing in Medical Imaging – IPMI 2008. LNCS, vol. 6801. 2011. p. 723–34.
[22] Schultz T, Seidel H-P. Estimating crossing fibers: a tensor decomposition approach. IEEE Trans Vis Comput Graph 2008;14(6):1635–42.
[23] Jiao F, Gur Y, Johnson C R, Joshi S. Detection of crossing white matter fibers with high-order tensors and rank-k decompositions. Information Processing in Medical Imaging. LNCS, vol. 6801. 2011. p. 538–49.
[24] Gur Y, Jiao F, Zhu S X, Johnson C R. White matter structure assessment from reduced hardi data using low-rank polynomial approximations. Medical image computing and computer-assisted intervention (MICCAI). 2012. p. 186.
[25] Megherbi T, Kachouane M, Oulebsir-Boumghar F, Deriche R. Crossing fibers detection with an analytical high order tensor decomposition. 18 pages Comput Math Methods Med1748-670X2014:476837https://doi.org/10.1155/2014/476837.
[26] Megherbi T, Ghosh A, Oulebsir-Boumghar F, Deriche R. Détection des croisements de fibres en irm de diffusion, in: Proceedings of the 3rd International Conference on image and signal processing and their applications (ISPA'12), December 2–4, 2012, in Mostaganem - Algeria, https://hal.archives-ouvertes.fr/hal-00989135/document.
[27] Bro R. PARAFAC. Tutorial and applications. Chemom Intell Lab Syst 1997;38:149–71.
[28] Ghosh A, Megherbi T, Oulebsir-Boumghar F, Deriche R. Fiber orientation distribution from non-negative sparse recovery. IEEE 11th International Symposium on Biomedical Imaging (ISBI2013): From Nano to Macro, San Francisco, CA, USA, April 8–11, 2013 1945-7928IEEE978-1-4673-6456-0; 2013. p. 254–7.http://ieeexplore.ieee.org/document/6556460/https://doi.org/10.1109/ISBI.2013.6556460. INSPEC Accession Number:13654392.
[29] Côté M-A, Girard G, Boré A, Garyfallidis E, Houde J-C, Descoteaux M. Tractometer: towards validation of tractography pipelines. Med Image Anal 2013;17(7):844–57.
[30] Tournier J D, Calamante F, Gadian D G, Connelly A. Direct estimation of the fibre orientation density function from diffusion-weighted MRI data using spherical deconvolution. J Multivar Anal 2004;23:1176–85.
[31] Healy D M, Hendriks H, Kim P T. Spherical deconvolution. J Multivar Anal 1998;67:1–22.
[32] Jeurissen B, Tournier J D, Dhollander T, Connelly A, Sijbers J. Multi-tissue constrained spherical deconvolution for improved analysis of multi-shell diffusion MRI data. Neuroimage 2014;26:103–411.
[33] Ghosh A, Deriche R. Greedy nnls: fiber orientation distribution from non-negatively constrained sparse recovery. Intl. Soc. Mag. Reson. Med. 22. 2014. p. 2610. Milan, Italy, May.
[34] Lawson CL, Hanson RJ. Solving least squares problems? Soc Ind Appl Math (SIAM) 1976;22(5).
[35] Daducci A, Caruyer E, Descoteaux M, Houde J-C, Thiran J-P. Hardi reconstruction challenge 2013. IEEE 11th International Symposium on Biomedical Imaging (ISBI). 2013.
[36] Van Essen D C, Smith S M, Barch D M, Behrens T E J, Yacoub E, Ugurbil K, et al. The WU-Minn human connectome project: an overview. NeuroImage 2013;80:62–79.
[37] Girard G, Whittingstall K, Deriche R, Descoteaux M. Towards quantitative connectivity analysis:reducing tractography biases. NeuroImage 2014;98:266–78.
[38] Garyfallidis E, Brett M, Amirbekian B, Rokem A, Van Der Walt S, Descoteaux M, et al. Dipy, a library for the analysis of diffusion MRI data. Front Neuroinform 2014;8:8.
[39] Tournier J-D, Calamante F, Connelly A. MRtrix: diffusion tractography in crossing fiber regions. Int J Imaging Syst Technol 2012;22(1):53–66.
[40] Caruyer E, Daducci A, Descoteaux M, Houde J-C, Thiran J-P, Verma R. Phantomas: a flexible software library to simulate diffusion mr phantoms. International Symposium on Magnetic Resonance in Medicine (ISMRM). 2014.
[41] Caruyer E, Lenglet C, Sapiro G, Deriche R. Design of multishell sampling schemes with uniform coverage in diffusion MRI Wiley Magn Reson Med 2013;69(6):1534–40.